8-2007

Wide-Field Survey of Globular Clusters in m31. I. a Catalog of New Clusters

Sang Chul Kim
Korea Astronomy and Space Science Institute; Seoul National University; Kitt Peak National Observatory, National Optical Astronomy Observatory

Myung Gyoon Lee
Seoul National University; Kitt Peak National Observatory, National Optical Astronomy Observatory

Doug Geisler
Kitt Peak National Observatory, National Optical Astronomy Observatory; Universidad de Concepción, Casilla

Ata Sarajedini
Kitt peak National Observatory, National Optical Astronomy Observatory; University of Florida, Gainesville

Hong Soo Park
Seoul National Univeristy

See next page for additional authors

The Astronomical Journal, 134:706 – 720, 2007 August

WIDE-FIELD SURVEY OF GLOBULAR CLUSTERS IN M31. I. A CATALOG OF NEW CLUSTERS

Sang Chul Kim,[1,2,3] Myung Gyoon Lee,[2,3] Doug Geisler,[3,4] Ata Sarajedini,[3,5] Hong Soo Park,[2]
Ho Seong Hwang,[2] William E. Harris,[6] Juan C. Seguel,[4,7] and Ted von Hippel[3,8,9]
Received 2007 January 27; accepted 2007 May 3

ABSTRACT

We present the result of a wide-field survey of globular clusters (GCs) in M31 covering a $3^\circ \times 3^\circ$ field centered on M31. We have searched for GCs on CCD images taken with Washington CMT_1 filters at the KPNO 0.9 m telescope using the following steps: (1) inspection of morphological parameters given by the SExtractor package such as stellarity, full width at half-maximum, and ellipticity; (2) consulting the spectral types and radial velocities obtained from spectra taken with the Hydra spectrograph at the WIYN 3.5 m telescope; and (3) visual inspection of the images of each object. We have found 1164 GCs and GC candidates, of which 605 are newly found GCs and GC candidates and 559 are previously known GCs. Among the new objects there are 113 genuine GCs, 258 probable GCs, and 234 possible GCs, according to our classification criteria. Among the known objects there are 383 genuine GCs, 109 probable GCs, and 67 possible GCs. In total there are 496 genuine GCs, 367 probable GCs, and 301 possible GCs. Most of these newly found GCs have T_1 magnitudes of 17.5–19.5 mag [$17.9 < V < 19.9$ mag assuming $(C - T_1) \approx 1.5$], and $(C - T_1)$ colors in the range 1–2.

Key words: galaxies: individual (M31, NGC 224) — galaxies: spiral — galaxies: star clusters — Local Group

Online material: color figures, machine-readable tables

1. INTRODUCTION

Globular clusters (GCs) are an ideal tool for studying the formation and evolution of nearby galaxies for several reasons. First, GCs are one of the brightest objects in galaxies, so it is relatively easy to observe them even in the outer parts of the galaxies where individual stars are too faint to be observed. Second, GCs are believed to be among the oldest objects in galaxies (see, e.g., Salaris & Weiss 2002; De Angeli et al. 2005), giving a lower limit to the ages of their parent galaxies. Third, the stars in GCs are believed to be born essentially at the same time and with the same chemical composition, which makes GCs an ideal laboratory for the study of stellar evolution. Fourth, GCs are distributed much more widely than stars, so they can be used for the study of the halo of their parent galaxy. Finally, since the present GCs have survived since the formation of their parent galaxies, they give information on the formation and evolution of both the clusters and the galaxies.

The GCs in M31 are especially important, since M31 is the nearest spiral galaxy and has an abundant population of GCs. There have been numerous studies of the GCs in M31 starting as early as 1932. Table 1 shows a list of the previous studies on M31 GCs, focusing primarily on the number of GCs and candidate GCs found. Examples of the most extensive GC surveys are those of Sargent et al. (1977; the M31 Consortium), Crampton et al. (1985; the DAO group), and Battistini et al. (1987; the Bologna group). However, these surveys are mostly based on visual searches of the photographic plates.

Since the use of CCD detectors in astronomy, there have been efforts to use them for deep photometry to search for new GCs in M31. However, the small field of view (FOV) of the first-generation CCDs enabled previous investigators only to perform GC surveys for a limited region of M31, and there has not yet been any wide-field survey of GCs using CCD cameras. It is clear from Table 1 that our new GC survey presented in this study is the first systematic one for the largest area of $\sim 3^\circ \times 3^\circ$ centered on M31.

Recently several new extended GCs were found in the halo located at 15 kpc $\lesssim R_p \lesssim$ 116 kpc (where R_p is the projected radius) from the center of M31 (Huxor et al. 2005; Martin et al. 2006; Mackey et al. 2007), and Mackey et al. (2006, 2007) presented deep photometry of stars in these clusters based on *Hubble Space Telescope* (*HST*) ACS images. Kodaira et al. (2004) found 49 compact star clusters with $M_V < -5$ mag and $0 < (B - V) < 1.0$ in the southwest field ($17.5' \times 28.5'$) of the M31 disk from CCD images taken at the Subaru 8 m telescope, some of which may be GCs.

This paper is the first in a series on our wide-field survey of M31 GCs. In this paper we present a catalog of new GCs in M31, and the analyses of the photometric and spectroscopic data of the new and known GCs in M31 will be presented in separate papers. Brief progress reports of this study were given in Lee et al. (2002), Kim et al. (2002), and Seguel et al. (2002), which are superseded by this series of papers.

This paper is organized as follows: § 2 describes the photometric and spectroscopic observations and data reductions, and § 3 the GC search method. Section 4 presents the catalog of new

[1] Korea Astronomy and Space Science Institute, Daejeon 305-348, Korea; sckim@kasi.re.kr.
[2] Astronomy Program, Department of Physics and Astronomy, Seoul National University, Seoul 151-742, Korea; mglee@astrog.snu.ac.kr, hspark@astro.snu.ac.kr, hshwang@astro.snu.ac.kr.
[3] Visiting Astronomer, Kitt Peak National Observatory, National Optical Astronomy Observatory, which is operated by the Association of Universities for Research in Astronomy (AURA), Inc., under cooperative agreement with the National Science Foundation.
[4] Grupo de Astronomia, Departamento de Fisica, Universidad de Concepción, Casilla 160-C, Concepción, Chile; dgeisler@astro-udec.cl, jseguel@andromeda.cfm.udec.cl.
[5] Department of Astronomy, University of Florida, Gainesville, FL 32611, USA; ata@astro.ufl.edu.
[6] Department of Physics and Astronomy, McMaster University, Hamilton, ON L8S 4M1, Canada; harris@physics.mcmaster.ca.
[7] Cerro Tololo Inter-American Observatory, Casilla 603, La Serena, Chile.
[8] Department of Astronomy, University of Texas at Austin, 1 University Station, C1400, Austin, TX 78712, USA; ted@astro.as.utexas.edu.
[9] Visiting Scientist, Southwest Research Institute, 1050 Walnut Street, Suite 400, Boulder, CO 80302, USA.

TABLE 1
A List of Previous M31 GC Searches

Reference	Plate vs. CCD	CCD FOV	N(GC)	Comments
Hubble (1932)	Plate	...	140	M31's disk only
Seyfert & Nassau (1945)	Plate	...	101	W. Baade's discovery, no coordinates
Vetešnik (1962)	Plate	...	(241)[a]	Coordinates, V magnitudes, and colors
Baade & Arp (1964)	Plate	...	30	
Mayall & Eggen (1953)	Plate	...	4	Outer parts of M31
Alloin et al. (1976)	Plate	...	5	Nuclear region of M31
Sargent et al. (1977)	Plate	...	355	KPNO 4 m
Crampton et al. (1985)	Spectra plates	...	109	CFHT 3.6 m; a catalog of total 509 GCs
Battistini et al. (1987)	Plate	...	353[b]	Bologna 1.52 m
Wirth et al. (1985)	Video camera	$2' \times 2'$	$\sim$50	Bulge region
Aurière et al. (1992)	CCD	$1.7' \times 2.7'$	16[c]	$7.7' \times 7.7'$ field centered on M31
Battistini et al. (1993)	CCD	320×512 pixel^2	4[d]	$R < 5.5'$ ($R \lesssim 1$ kpc)
Mochejska et al. (1998)	CCD	$11' \times 11'$	4[e]	Four fields in M31's disk
Barmby et al. (2000)	CCD	$22' \times 22'$	(435)[f]	A new catalog of "best" photometry
Barmby & Huchra (2001)	*HST* WFPC2	$\sim 2.7' \times 2.7'$	32	157 images
Perrett et al. (2002)	Spectroscopy	...	(288)[g]	WHT 4.2 m + WYFFOS
Galleti et al. (2004)	2MASS/NICMOS3	All sky	(693)[h]	Revised Bologna Catalog of 1035 objects
Huxor et al. (2005)	CCD	≈ 0.29 deg^2	3	INT 2.5 m + WFC
Galleti et al. (2006)	Spectroscopy	...	(42)[i]	Revised Bologna Catalog, ver. 2.0
Mackey et al. (2006); Mackey et al. (2007)	*HST* ACS	$\sim 3.4' \times 3.4'$	14	*HST* Program GO 10394 (Cycle 13)
This study	CCD	$23.2' \times 23.2'$	605[j]	Mapping $\sim 3^\circ \times 3^\circ$ field centered on M31

[a] Not new discoveries, but studies on the objects found by Hubble (1932) and Seyfert & Nassau (1945).
[b] With 254 class A, 99 class B, 152 class C, and 218 class D objects, where class A objects are very high confidence objects, class B objects are high-confidence objects, class C objects are plausible candidates, and class D miscellaneous nonstellar objects with an expected percentage of actual clusters of the order of a few percent.
[c] With 12 reliable, 4 possible.
[d] With 3 class A, 1 class B, 20 class C, and 20 class D objects.
[e] With 2 class A, 2 class B, 28 class C, and 36 class D objects.
[f] Observations of 13 fields centered on M31, but no GC search. Of the 435 objects, 268 have optical photometry in four or more filters, 224 have near-infrared photometry, 200 have radial velocities, and 188 have spectroscopic metallicities.
[g] Spectroscopy for 288 previously known objects. They presented a spectroscopic database of 321 velocities and 301 metallicities.
[h] 2MASS near-infrared photometry for 693 known and candidate GCs. Of 1035 objects, 337 are confirmed GCs, 688 are GC candidates, and 10 are objects with controversial classification.
[i] Confirmed GC nature from spectroscopy of 76 candidates.
[j] With 113 class 1, 258 class 2, and 234 class 3, where classes 1, 2, and 3 are similar to classes A, B, and C, respectively, in Battistini et al. (1987).

GCs found in this study and some properties of newly found GCs, and finally, a summary is given in § 5.

2. OBSERVATIONS AND DATA REDUCTION

We carried out two kinds of observation for the survey of M31 GCs. First, photometric observations were made using the CCD camera at the KPNO 0.9 m telescope. Second, spectroscopic observations were performed using the Hydra multifiber spectrograph at the WIYN 3.5 m telescope. We describe the details of these observations below.

2.1. *Photometry*

2.1.1. *Observation*

We obtained Washington C and M and broadband Kron-Cousins R images using the T2KA CCD camera at the KPNO 0.9 m telescope on the nights of UT 1996 October 14–25 and UT 1998 October 19. The pixel scale of the CCD chip is $0.68''$ pixel^{-1}, and the CCD has 2048×2048 pixels, corresponding to $23.2' \times 23.2'$ on the sky. We used the Kron-Cousins R filter as an alternative to the T_1 filter, since the R filter accurately reproduces the T_1 photometry with 3 times greater efficiency (Geisler 1996). The resulting calibrated magnitudes and colors will therefore be in the Washington CMT_1 system. Geisler (1996) gave a transformation relation between R and T_1, $R = 0.003 + T_1 - 0.017(C - T_1)$, with an rms of only 0.02 mag derived from the data of 53 standard stars.

We observed 53 fields covering the central region of M31. Figure 1 shows the location of the observed fields, the names of which are labeled in the upper left corner of each solid box. For most of the fields, one exposure per filter was made. Typical exposure times for the 1996 run were 1500 s for C and 600 s for M and R, while those for the 1998 run were 1200 s for C and 500 s for M and R. The seeing was mostly $1.1''$–$2.0''$ (1.6–2.9 pixels in our CCD frames) during the observations, although a few fields have a seeing of $2.0''$–$3.0''$. Table 2 lists the journal of observation, where column (1) is the night number, column (2) the observation date in UT, column (3) the field numbers, and column (4) the weather condition. Of the total of 11 nights of observation, four nights (N5, N8, N9, and Oct98) were photometric, three (N3, N4, and N11) were semiphotometric, and the remaining four nights were nonphotometric or even cloudy. The standard star observations were made in the photometric and semiphotometric nights indicated in Table 2.

2.1.2. *Data Reduction*

We processed all the CCD images to apply overscan correction, bias subtraction, and flat-fielding using the IRAF[10] CCDRED package. We derived the calibration transformation using the Washington standard stars (Geisler 1996) observed during the observing runs. We obtained the aperture magnitudes of the standard

[10] IRAF (Image Reduction and Analysis Facility) is distributed by the National Optical Astronomy Observatory, which is operated by AURA, Inc., under cooperative agreement with the National Science Foundation.

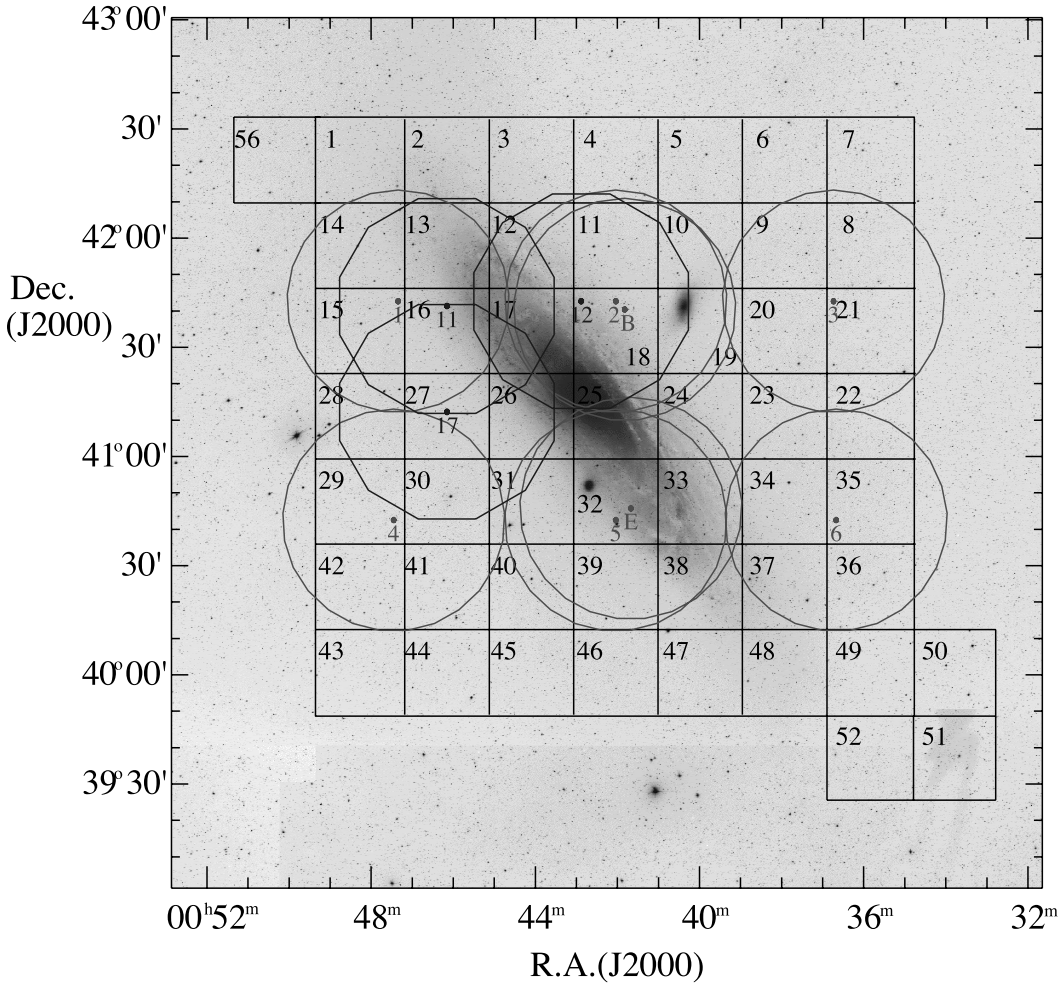

FIG. 1.—Locations of our survey regions overlaid on a $4^\circ \times 4^\circ$ optical image of M31 from the Digitized Sky Survey (image center: R.A. = $0^h42^m15^s$, decl. = $+41^\circ00'37''$ [J2000.0]). North is at the top, and east is to the left. The fields for the KPNO 0.9 m photometric imaging are drawn with solid boxes with the field names labeled in the upper left corner of each box. The field of view of each field is $23.2' \times 23.2'$, and the observations were made so that there was some ($1'-2'$) overlap between adjacent fields. Satellite galaxies NGC 205 and M32 are located in fields 19 and 32, respectively. The Hydra fields are denoted by smooth circles (for 2000) and polygon-like circles (for 2001), and their names are labeled near the center of each field. [*See the electronic edition of the Journal for a color version of this figure*.]

TABLE 2

SUMMARY OF KPNO 0.9 m PHOTOMETRIC OBSERVATIONS

Night[a] (1)	Obs. Date (UT) (2)	Field (3)	Weather (4)
N1	1996 Oct 14	23(C), 26	Cloudy
N2	1996 Oct 15	16, 17, 18(long)[b], 19, 20, 23(M, T_1), 24, 25(long)[c], 27	Cloudy
N3*	1996 Oct 16	18(short),[b] 25(short),[c] 30, 31, 32, 33, 34, 35	Semiphotometric
N4*	1996 Oct 17	28, 36	Semiphotometric
N5*	1996 Oct 18	09, 10, 37, 38, 39, 40, 41	Photometric
N6	1996 Oct 19	...	...
N7	1996 Oct 20	...	...
N8*	1996 Oct 21	11, 12, 13, 14, 15, 29, 42, 43(M)	Photometric
N9*	1996 Oct 22	43(C, T_1), 44, 45[d]	Photometric
N10	1996 Oct 23	(45[d]), 46, 47, 48, 49, 50	Nonphotometric
N11*	1996 Oct 24	01, 02, 03, 04, 05	Semiphotometric
N12	1996 Oct 25	06	Nonphotometric
Oct98*	1998 Oct 19	07, 08, 21, 22, 51, 52, 56	Photometric

[a] Asterisks indicate nights on which standard transformation data (photometric and semi-photometric nights) were obtained.

[b] For the field of F18, which is just the northern field of F25, we took two sets of data: long exposures (1500 s in C, 600 s in M, and 600 s in T_1) and short exposures (300 s in C, 100 s in M, and 100 s × 2 in T_1).

[c] For the field of F25, which includes the M31 central region, we took two sets of data: long exposures (1500 s in C, 600 s in M, and 300 s × 2 in T_1) and short exposures (300 s in C, 200 s in M, and 200 s × 2 in T_1).

[d] Field 45 was observed on both N9 and N10 with the same exposure time setups. Even though the seeing of N10 for F45 was slightly better than that of N9 (1.6″ vs. 2.0″), we primarily used the N9 data for the utilization of N9 standard transformation information.

TABLE 3
SUMMARY OF WIYN 3.5 m SPECTROSCOPIC OBSERVATIONS

Obs. Date (UT)	Hydra Configuration	N(observed)[a] (=new[b] + old[c])	N(vel)[d]	Exposure Time
2000 Sep 7	1	68 (=66+2)	38	1800 s × 4 = 7200 s (2 hr)
2000 Sep 7	2	73 (=56+17)	66	1800 s × 3 + 900 s = 6300 s (1 hr 45 minutes)
2000 Sep 8	3	64 (=64+0)	47	1800 s × 4 = 7200 s (2 hr)
2000 Sep 8	4	62 (=59+3)	34	1800 s × 3 = 5400 s (1 hr 30 minutes)
2000 Sep 8	5	71 (=59+12)	56	1800 s × 4 = 7200 s (2 hr)
2000 Sep 9	6	75 (=74+1)	36	1800 s × 4 = 7200 s (2 hr)
2000 Sep 9	B	70 (=67+3)	56	1800 s × 4 = 7200 s (2 hr)
2000 Sep 9	E	70 (=60+10)	57	1800 s × 3 + 1041 s = 6441 s (1 hr 47 minutes 21 s)
Subtotal		552 (=504+48)	390	
2001 Nov 2	11	69 (=54+15)	35	2400 s × 3 = 7200 s (2 hr)
2001 Nov 2	12	79 (=45+34)	60	2400 s × 3 = 7200 s (2 hr)
2001 Nov 2	17	47 (=38+9)	20	2400 s × 1 = 2400 s (40 minutes)
Subtotal		195 (=137+58)	115	
Total		748 (=642+106)	505	

[a] Number of all observed objects.
[b] GC candidates found from the photometric criteria in this study.
[c] Previously known GCs.
[d] Number of objects for which successful velocities were measured.

stars using a 7.5″ radius aperture (the same as in Geisler 1996) from the images of the standard stars. Then we used the IRAF PHOTCAL package to derive the calibration equations.

For three out of the four nights of photometric conditions, all three standard calibration coefficients (zero point, color term, and air-mass term) were derived. For the three nights of semi-photometric conditions, we adopted the mean values of the color and air-mass term coefficients of the three photometric nights to derive the zero points. Although the night of UT 1996 October 22 was believed to be photometric, there were not enough standard stars to derive all three calibration coefficients independently, so we adopted the color and air-mass term coefficients of the previous photometric night.

For the fields observed on the nights without standard stars, we derived secondary standard transformations using the neighboring fields. Since we initially arranged our target fields to overlap adjacent fields by 1′–2′, we could easily identify the stars in common between two neighboring fields. On the image of each filter, we first identified the positions of the common stars in the two adjacent fields, calculated the mean magnitude offsets between the standardized magnitudes and instrumental magnitudes, and then applied this magnitude offset (together with the color and atmospheric coefficients of the standardized field) to transform the instrumental magnitudes of the nonphotometric frames. There are 14 fields for which this secondary transformation method is applied. The typical errors of the standard star calibration are 0.020, 0.022, and 0.019 mag for T_1, $(C - T_1)$, and $(M - T_1)$, respectively.

We have derived the photometry of the objects in the target images using the SExtractor package (Bertin & Arnouts 1996). SExtractor performs detection of objects in the images and gives position, aperture magnitude, stellarity, the full width at half-maximum (FWHM), ellipticity, position angle, quality of the photometry, and some other parameters. We used the SExtractor parameters DETECT_MINAREA = 5 pixel and DETECT_THRESH = 1.5 σ above the local background. The results for new GC searches do not depend strongly on the choice of these values. The instrumental magnitudes of the objects obtained using the SExtractor package were transformed into the standard system using the calibration equations.

We have obtained plate solutions for each of the CCD images for astrometry of objects using the Guide Star Catalogue (GSC) provided by the Space Telescope Science Institute (STScI) and the IRAF tasks `ccxymatch` and `ccmap`.

These plate solutions transform the X and Y coordinates of our R images to/from the celestial equatorial coordinates of epoch J2000.0 by using the IRAF `cctran` task. The mean rms errors in right ascension and declination are $0.064'' \pm 0.023''$ and $0.064'' \pm 0.024''$, respectively.

2.2. *Spectroscopy*

2.2.1. *Observation*

For most of the GC candidates selected from the photometric list of the objects to be described in the next section, we carried out spectroscopic observation using the Hydra multifiber bench spectrograph and T2KC CCD at the WIYN 3.5 m telescope on the nights of UT 2000 September 7–9 and UT 2001 November 2–4. Table 3 lists the journal of spectroscopic observations. Table 3 shows the observation date in UT, the number of target objects, and the exposure time for each Hydra configuration marked in Figure 1.

For both the 2000 and 2001 observations, almost the same instrumental setup was used. The 400 lines mm^{-1} at 4.2° blaze angle grating and Simmons camera were used. This combination with the blue fiber cable covers a wavelength range of ~3400–6600 Å in the first order and gives a 7.07 Å spectral resolution and 1.56 Å pixel^{-1} dispersion.

During the observing run of 2000, all three nights were clear and a total of eight Hydra configurations were used for spectroscopy. However, in the run of 2001 only the first night was clear, while the two subsequent nights were cloudy or rainy. Only three Hydra configurations were obtained during this run. The total number of targets observed during the observing runs was 748, including 106 previously known GCs observed in order to quantify our errors and compare our values with previous studies.

2.2.2. *Data Reduction*

First we performed overscan correction, image trimming, bias subtraction, and flat combining on the spectroscopic data using the IRAF CCDRED package. We removed cosmic rays in the object images and combined the resulting object images. For the reduction of the Hydra spectroscopic data, we used the Hydra

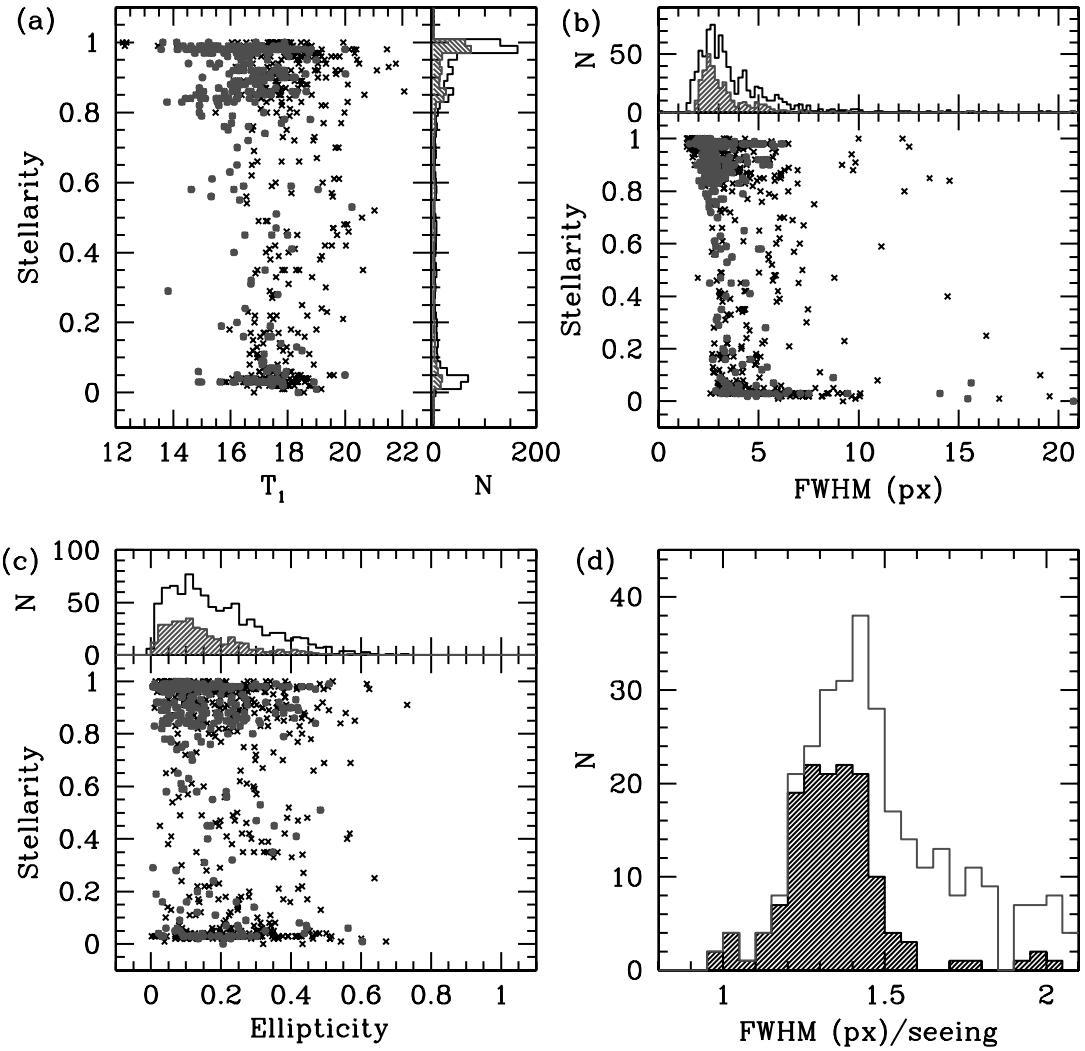

FIG. 2.—SExtractor parameter distributions of the 347 confirmed and 514 candidate GCs in the catalogs of Galleti et al. (2006; RBC2), Huxor et al. (2005), and Mackey et al. (2007) matched with our photometry. (*a*) Stellarity vs. T_1 magnitude; (*b*) stellarity vs. FWHM; (*c*) stellarity vs. ellipticity; (*d*) histogram of FWHM/seeing distribution. In panels *a*, *b*, and *c*, the crosses and the open solid histograms show the distributions of all 861 objects with good photometry, and the filled circles and hatched histograms show those of the 347 confirmed GCs. In panel *d*, the open solid histogram shows the distribution of the 347 confirmed GCs, and the hatched histogram the 147 confirmed compact GCs with stellarity >0.95. [*See the electronic edition of the Journal for a color version of this figure.*]

data reduction task, IRAF DOHYDRA, which was specifically designed for multifiber spectral reduction (Valdes 1995).

Before doing the main data reduction part, DOHYDRA first performs aperture finding using the `apfind` task, and performs fitting and subtracting of the scattered light using the `apscatter` task. Then DOHYDRA performs aperture extraction, flat-fielding, fiber throughput correction, wavelength calibration, and sky subtraction. Dome-flat images were used as a template to extract the one-dimensional object and calibration spectra from the two-dimensional images. Cu/Ar calibration lamp spectra were used for wavelength calibration. The rms error of the wavelength calibration is estimated to be typically 0.2–0.3 Å. Finally, we calibrated the flux of the spectra of the targets using the spectra of the flux standard star BD +40 4032 (R.A. $= 20^{\rm h}06^{\rm m}40.0^{\rm s}$, decl. $= +41^\circ06'15''$ [B1950.0], B2 III, $m_{5556} = 10.45$ mag; Strom 1977) using the `calibrate` task.

We determined the radial velocity of the targets by cross-correlating their spectra against high signal-to-noise ratio (S/N) template spectra using the IRAF `fxcor` task (Tonry & Davis 1979; Huchra et al. 1991). We used two bright GCs in M31 as a reference. GCs 020-073 and 158-213 are relatively bright clusters with $V = 14.91$ mag and $(B - V) = 0.83$, and $V = 14.70$ mag and $(B - V) = 0.86$, respectively, and have well-determined radial velocities of $V_r = -349 \pm 2$ and -183 ± 4 km s^{-1}, respectively (Barmby et al. 2000). We used the wavelength range of 3900–5400 Å for velocity measurement, excluding the noisy region of $\lambda > 5500$ Å due to some sky lines not completely eliminated even after sky subtraction. Measuring errors of the radial velocity are typically err(v) = 35 km s^{-1}. For the objects with successfully measured velocity values, we measured the S/N values at $\lambda \sim 5000$ Å, obtaining $1 < {\rm S/N} < 75$. The peak S/N values are 6–10 for all these spectra, and 10–20 for newly found, highest probability GCs.

3. CLUSTER SEARCH METHOD

We have used both photometric and spectroscopic information to select GCs in M31. First, using photometric data, we investigated various photometric parameters and morphological properties of the objects in the CCD images. Then we assigned spectral classes to bright objects, and used the radial velocities to determine the M31 membership of the objects with measured radial velocities. Finally, we performed the final classification by careful visual inspection of the image of each object, after training our eyes with images of the previously known GCs, stars, and

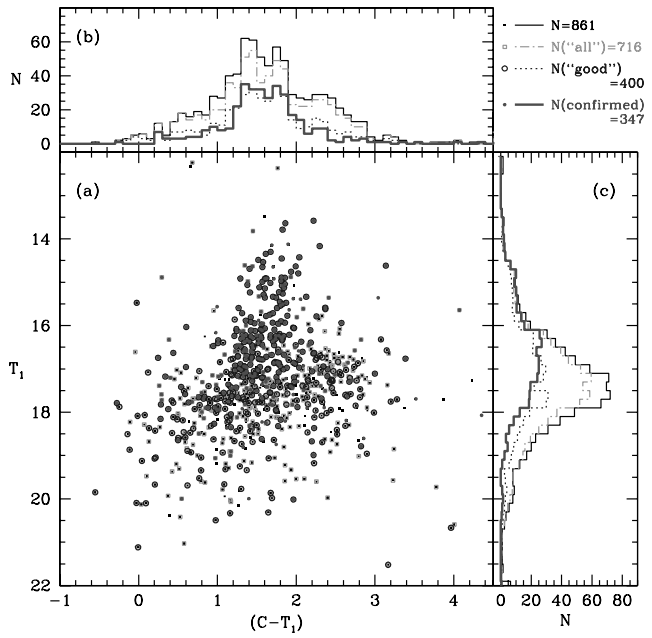

FIG. 3.—(*a*) Color-magnitude diagram; (*b*) $(C - T_1)$ color distribution; (*c*) T_1 LF of the 347 confirmed and 514 candidate GCs in the catalogs of Galleti et al. (2006; RBC2), Huxor et al. (2005), and Mackey et al. (2007) matched with our photometry. Small dots and thin solid histograms show the distributions of all 861 objects with good photometry, open squares and dot-dashed histograms show the distributions of "all GC candidates" from the GC search criterion 1, open circles and dotted histograms show the distributions of "good GC candidates" from criterion 2, and filled circles and thick solid histograms show the distributions of the confirmed GCs in the three papers above. [*See the electronic edition of the Journal for a color version of this figure*.]

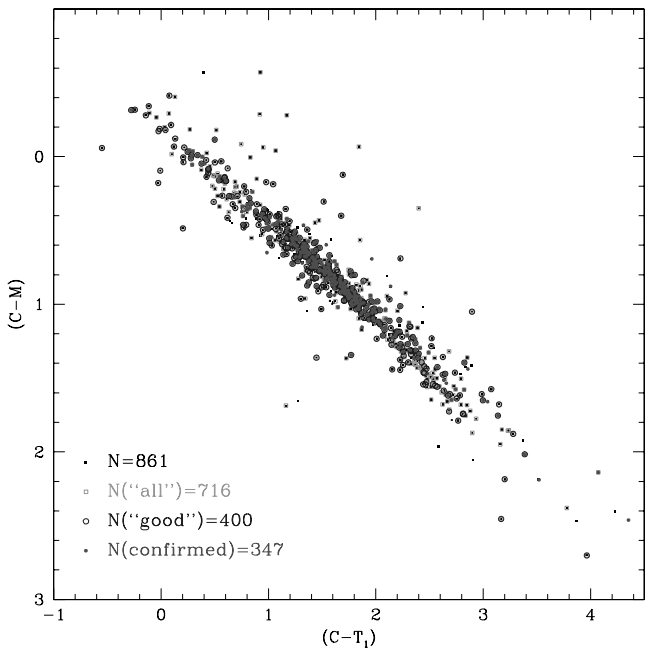

FIG. 4.—Color-color diagram of the 347 confirmed and 514 candidate GCs in the catalogs of Galleti et al. (2006; RBC2), Huxor et al. (2005), and Mackey et al. (2007) matched with our photometry. Small dots show the distributions of all 861 objects with good photometry, open squares show the distributions of "all GC candidates" from the GC search criterion 1, open circles show the distributions of "good GC candidates" from criterion 2, and filled circles show the distributions of the confirmed GCs in the three papers above. [*See the electronic edition of the Journal for a color version of this figure*.]

galaxies in our own data. Details of these steps are described below.

Before starting a survey of M31 GCs, we tried to find the suitable parameter space to select M31 GC candidates using the photometric data of the known M31 GCs. We matched our photometric catalog of the objects with the previous catalogs of Galleti et al. (2006; Revised Bologna Catalog, ver. 2.0 [RBC2]—their confirmed and candidate GCs), Huxor et al. (2005), and Mackey et al. (2007). There are 861 objects (347 confirmed GCs and 514 GC candidates) common between the previous catalogs and our catalog of photometry derived from our CCD images.

Figure 2 shows the distributions of three SExtractor parameters (stellarity, FWHM, and ellipticity) based on the *R* images, and Figures 3 and 4 show the photometric diagrams of these objects. In Figures 2*a*, 2*b*, and 2*c*, the crosses and the open solid histograms show the distributions of all 861 objects with good photometry, and the filled circles and hatched histograms show those of the confirmed GCs in common between this study and the papers above. A stellarity of 1 corresponds to a point source (star), and a stellarity of 0 to a resolved object. The distribution of stellarity in Figure 2 shows that most objects have stellarity of 1, few objects have stellarity between 0.1 and 0.8, and the rest have stellarity $\sim$0. Figure 2*d* shows the histogram of the normalized FWHM, which is the measured FWHM divided by the seeing value of each image.

In Figure 2 several features are noted: (1) the distribution of the stellarity of the confirmed GCs shows a strong peak around 1 with a broad tail extending to about 0.8, and a weak peak around 0. There are relatively much fewer GCs in the range between 0.1 and 0.8; (2) the distribution of the ellipticity of the confirmed GCs shows a broad peak around 0.1 with a tail extending to 0.5; and (3) the distribution of the normalized FWHM of the confirmed GCs shows a strong peak around 1.4, which is significantly larger than that of the stars, 1.0. Considering the pixel scale of our CCD chip, typical seeing of 2 pixels ($\approx$1.4″), and the linear size of 1″ at the distance of M31 ($\approx$3.78 pc), it is expected that most of the GCs in M31 will appear point-source-like. Even for these star-like GCs, Figure 2*d* shows that the normalized FWHM is greater than 1.

Considering the features in Figure 2, we have set up two kinds of criteria for the selection of GC candidates: (1) criteria for "all candidates" are (*a*) all values of stellarity, (*b*) $1.15 <$ FWHM/seeing $\lesssim$10, and (*c*) ellipticity $<$0.7; and (2) criteria for "good candidates" are (*a*) stellarity of 0.8–1.0, (*b*) $1.15 <$ FWHM/seeing $\lesssim$5, and (*c*) ellipticity $<$0.5. "Good candidates" are candidates with higher probability among "all candidates." Figure 3 shows the T_1-$(C - T_1)$ color-magnitude (CM) diagram (Fig. 3*a*), the histograms of $(C - T_1)$ color (Fig. 3*b*), and T_1 magnitude (Fig. 3*c*) of the 861 objects matched with the previous catalogs. Figure 4 shows the $(C - M)$-$(C - T_1)$ color-color (CC) diagram of the same objects. Notable features in Figures 3 and 4 are that (1) the colors of the confirmed GCs are mostly in the range $1 < (C - T_1) < 2$, (2) the luminosity function (LF) of the confirmed GCs shows a peak at $T_1 \approx 17$ mag, (3) the CM diagram shows a dominant vertical plume of GCs with $1 < (C - T_1) < 2$ extending up to $T_1 \sim 13.5$, and (4) the CC diagram shows a well-defined linear sequence of star clusters.

In Figures 3 and 4 we also plotted the data for "all candidates" and "good candidates." It is striking that the general properties of these candidates seen in these figures are very similar to those of the confirmed GCs, noting that no information of color and magnitude was used for selecting these candidates. This indicates that a significant fraction of these candidates may be GCs.

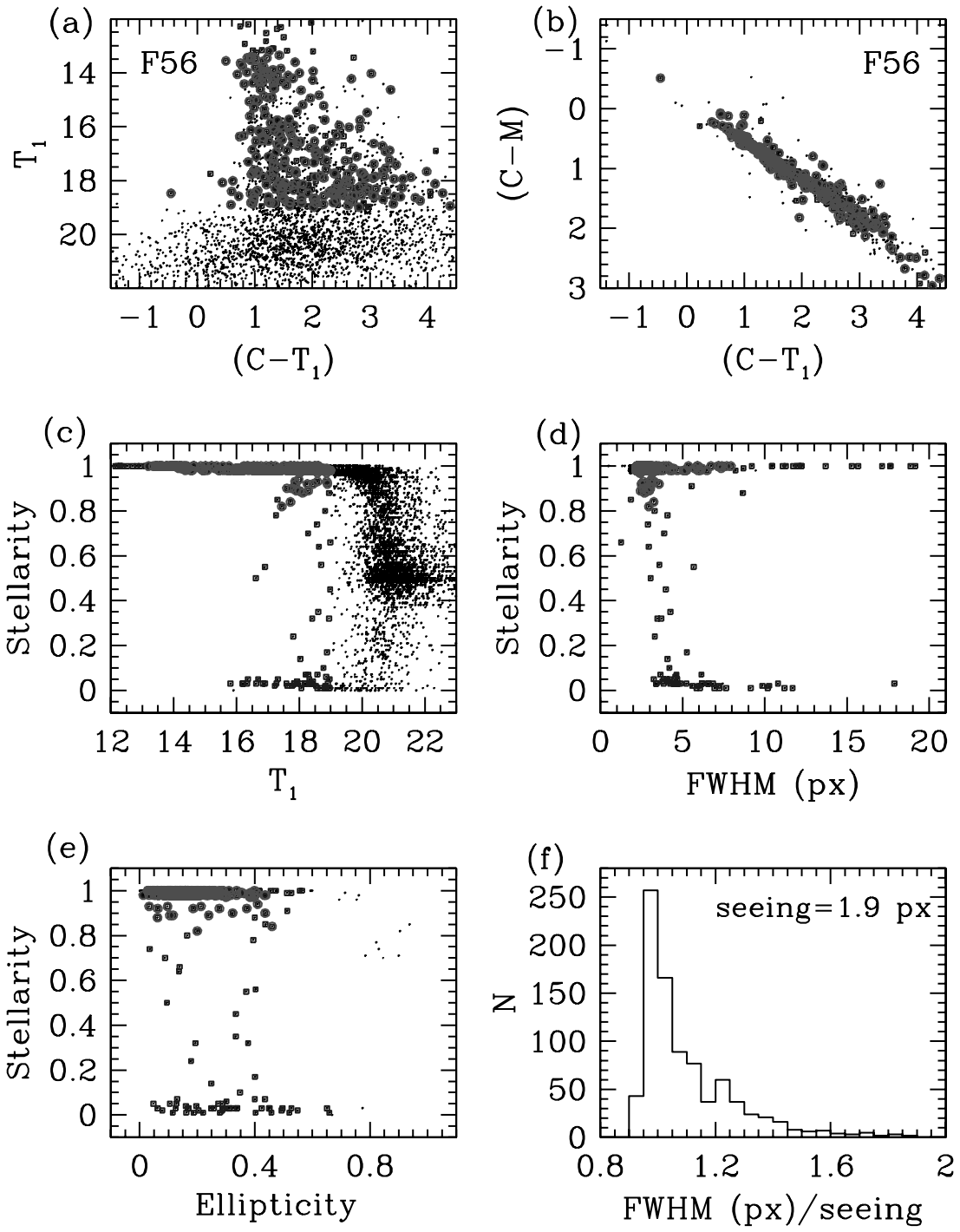

FIG. 5.—Example of our application of the GC search criteria to one of the KPNO fields (F56) with seeing of ≈1.9 pixels. Panels *a* and *b* show the CM diagram and CC diagram of the selected GC candidates, respectively, and panels *c*–*f* show the parameter space for the GC candidate selection (see § 3 for details). Small dots represent all measured objects with good photometry ($N = 4894$), squares represent "all GC candidates" selected according to criterion 1 ($N = 362$), and open circles superimposed on the squares represent "good GC candidates" selected according to criterion 2 ($N = 277$). [*See the electronic edition of the Journal for a color version of this figure*.]

We selected the candidates in the best-seeing image among the C, M, and R images, which are predominantly the R-band images. We used objects at least ∼1 mag brighter than the limiting magnitude where the stellarity cannot be used to separate stellar/nonstellar objects. The typical limiting magnitude of the images is $T_1 = 22$–23 mag, varying from field to field due to the seeing and the crowding in the field. We set the magnitude cut-off value for the candidate selection 1–2 mag brighter than the limiting magnitude of the images, depending on the seeing and the crowding in the images. The magnitude cut-off value for the candidate selection ranges from $T_1 \sim 17.5$ mag (for the center field) to ∼19.5 mag (for halo fields or good seeing), mostly $T_1 \sim 19$ mag. Therefore, our search is considered to be incomplete at $T_1 > 19$ mag for most fields (at $T_1 > 17.5$ mag for the central field). Figure 5 shows an example of our application of the above criteria to one of the KPNO fields (F56) with a seeing of ≈1.9 pixels. In this field, there are 4894 measured objects with good photometry. Among these we selected 362 "all GC candidates"

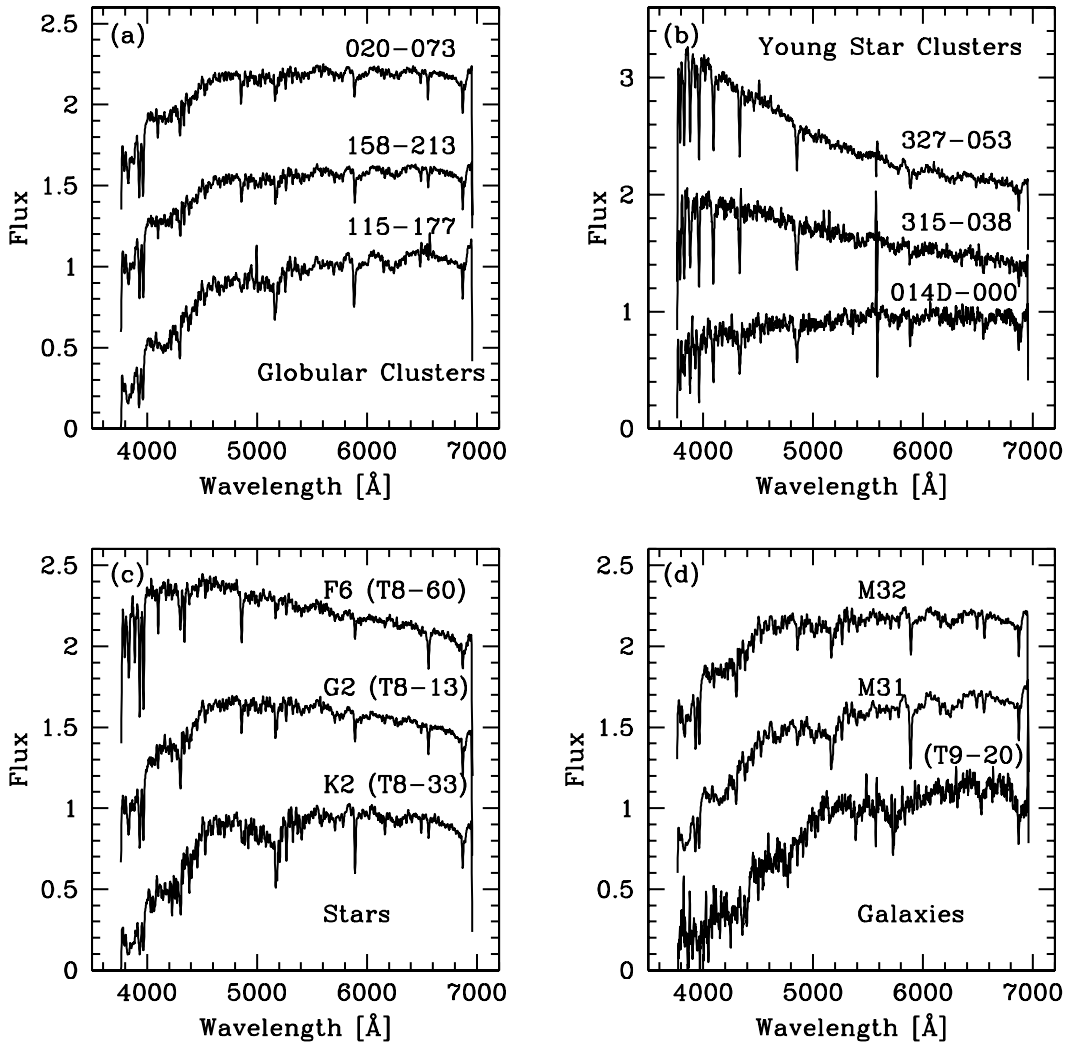

FIG. 6.—Sample spectra of (*a*) M31 globular clusters, (*b*) M31 young star clusters, (*c*) foreground stars, and (*d*) three galaxies (M31, M32, and a background galaxy). We have followed Huchra et al. (1991) and Barmby et al. (2000) for the naming convention of M31 GCs. The numbers after T8- and T9- in the parentheses of panels *c* and *d* are the identification numbers in Tables 8 and 9, respectively.

according to criterion 1 and 277 "good GC candidates" according to criterion 2.

Finally, we marked the "all" and "good" GC candidates selected above on the images, and visually inspected their images to finalize the GC candidates. We checked contour maps and radial profiles of the objects, as well as the images themselves. In the contour maps, we classified irregular, significantly elongated, asymmetric, and loosely concentrated objects as galaxies, and round, slightly elongated, strongly concentrated objects as star clusters. Although some faint galaxies look round in the displayed images, in the contour maps their outer areas look irregular, while star clusters look very smooth and round. Inspection of the contour maps was very efficient in selecting galaxies. In the radial profile, the objects with FWHM larger than the seeing size are considered as GCs, those with FWHM similar to seeing size as stars, and those with a large excess in the wing as galaxies. Checking color, position, and/or velocity information was also included. There are some confusing cases: compact elliptical galaxies versus GCs, compact GCs versus stars, and compact star clusters in H II regions versus galaxies. For these cases spectroscopic information was needed for classification. In the outer areas close to the edge of each CCD image, the FWHMs get larger due to image degradation. Therefore, we carefully compared potential targets in these areas with other nearby objects to see whether they are really extended.

Spectral information was also used for the classification of bright objects. We have visually classified the flux-calibrated spectra into stars, star clusters, and galaxies, comparing them with the template spectra of the spectral library of Santos et al. (2002). We used the continuum of the 4000–7000 Å wavelength range, as well as various spectral features: Balmer lines between 4000 and 5000 Å for early-type objects; absorption lines like Ca II H and K, CH (G band), Mg H+Mg *b*, and TiO for late-type objects; and emission lines for galaxies. Figure 6 displays sample spectra for

TABLE 4
NUMBER OF GLOBULAR CLUSTERS FOUND IN THIS STUDY

Class	Previously Found by Others[a]	New GCs	Sum
1.....	383	113	496
2.....	109	258	367
3.....	67	234	301
Sum	559	605	1164

[a] In Huxor et al. (2005), Galleti et al. (2006), Mackey et al. (2007), and references therein.

TABLE 5

A List of New Globular Clusters (Class 1)

ID (1)	R.A. (J2000.0) (2)	Decl. (J2000.0) (3)	T_1 (4)	$(M - T_1)$ (5)	$(C - T_1)$ (6)	v (km s^{-1}) (7)
1.....	00 36 33.54	+40 39 44.3	17.251 ± 0.007	0.650 ± 0.011	1.542 ± 0.015	−239.5 ± 46.7
2.....	00 36 34.99	+41 01 08.0	18.805 ± 0.030	0.677 ± 0.047	1.407 ± 0.060	−402.7 ± 92.5
3.....	00 37 10.67	+41 41 17.4	17.834 ± 0.011	0.778 ± 0.019	1.787 ± 0.030	−315.9 ± 34.5
4.....	00 38 01.31	+42 04 06.0	18.311 ± 0.016	0.708 ± 0.027	1.565 ± 0.040	−27.4 ± 32.8
5.....	00 38 59.15	+41 40 27.4	18.848 ± 0.031	0.877 ± 0.077	1.842 ± 0.083	−405.2 ± 43.1

Notes.—Table 5 is published in its entirety in the electronic edition of the *Astronomical Journal*. A portion is shown here for guidance regarding its form and content. Units of right ascension are hours, minutes, and seconds, and units of declination are degrees, arcminutes, and arcseconds.

TABLE 6

A List of New Probable Globular Clusters (Class 2)

ID (1)	R.A. (J2000.0) (2)	Decl. (J2000.0) (3)	T_1 (4)	$(M - T_1)$ (5)	$(C - T_1)$ (6)	v (km s^{-1}) (7)
1.....	00 33 23.07	+40 04 40.7	17.784 ± 0.015	0.896 ± 0.036	2.223 ± 0.102	...
2.....	00 33 32.20	+39 51 32.8	17.534 ± 0.010	0.505 ± 0.014	1.009 ± 0.014	...
3.....	00 33 37.03	+39 40 59.0	16.283 ± 0.004	0.794 ± 0.006	1.570 ± 0.007	...
4.....	00 34 34.20	+40 02 49.4	18.777 ± 0.038	1.145 ± 0.106	2.277 ± 0.266	...
5.....	00 35 21.20	+41 55 32.6	17.957 ± 0.013	1.031 ± 0.025	2.646 ± 0.065	...

Notes.—Table 6 is published in its entirety in the electronic edition of the *Astronomical Journal*. A portion is shown here for guidance regarding its form and content. Units of right ascension are hours, minutes, and seconds, and units of declination are degrees, arcminutes, and arcseconds.

TABLE 7

A List of New Possible Globular Clusters (Class 3)

ID (1)	R.A. (J2000.0) (2)	Decl. (J2000.0) (3)	T_1 (4)	$(M - T_1)$ (5)	$(C - T_1)$ (6)	v (km s^{-1}) (7)
1.....	00 33 13.08	+40 05 26.0	18.219 ± 0.023	0.990 ± 0.057	1.998 ± 0.127	...
2.....	00 33 15.82	+40 00 24.7	18.018 ± 0.019	0.968 ± 0.046	2.502 ± 0.159	...
3.....	00 33 34.43	+40 11 06.5	17.231 ± 0.009	0.897 ± 0.022	2.013 ± 0.052	...
4.....	00 33 34.96	+40 08 16.3	18.523 ± 0.030	1.166 ± 0.087	1.233 ± 0.093	...
5.....	00 33 38.04	+39 35 35.7	18.067 ± 0.015	1.182 ± 0.032	2.798 ± 0.069	...

Notes.—Table 7 is published in its entirety in the electronic edition of the *Astronomical Journal*. A portion is shown here for guidance regarding its form and content. Units of right ascension are hours, minutes, and seconds, and units of declination are degrees, arcminutes, and arcseconds.

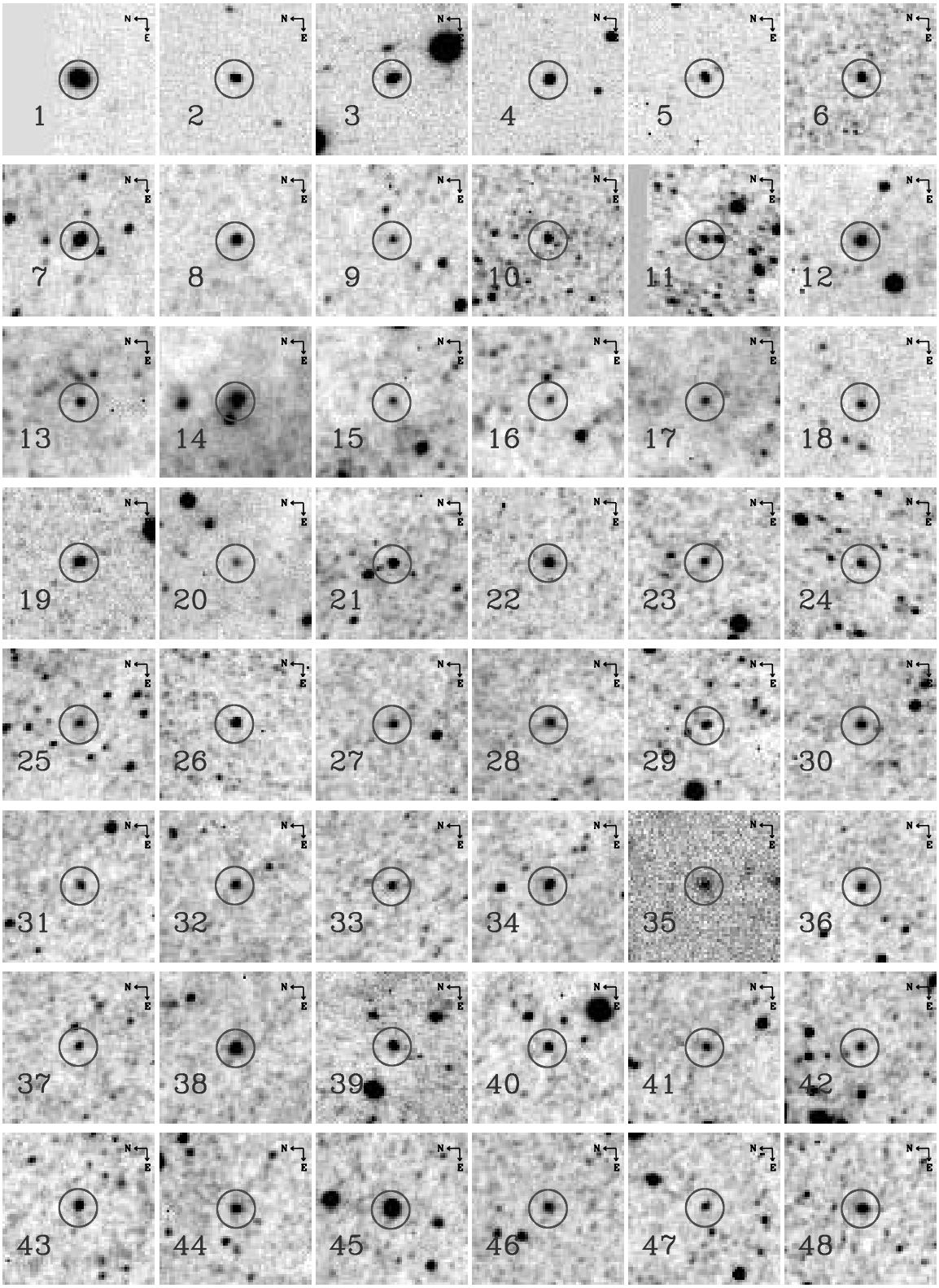

FIG. 7.—Gray-scale mosaic maps of the *R*-band CCD images of genuine GCs (class 1) for identifications from 1 to 48 in Table 5. The size of each field is $40'' \times 40''$, with north to the left and east at the bottom. The GC is centered in each image, in the center of the circle of $5''$ radius. [*See the electronic edition of the Journal for a color version of this figure*.]

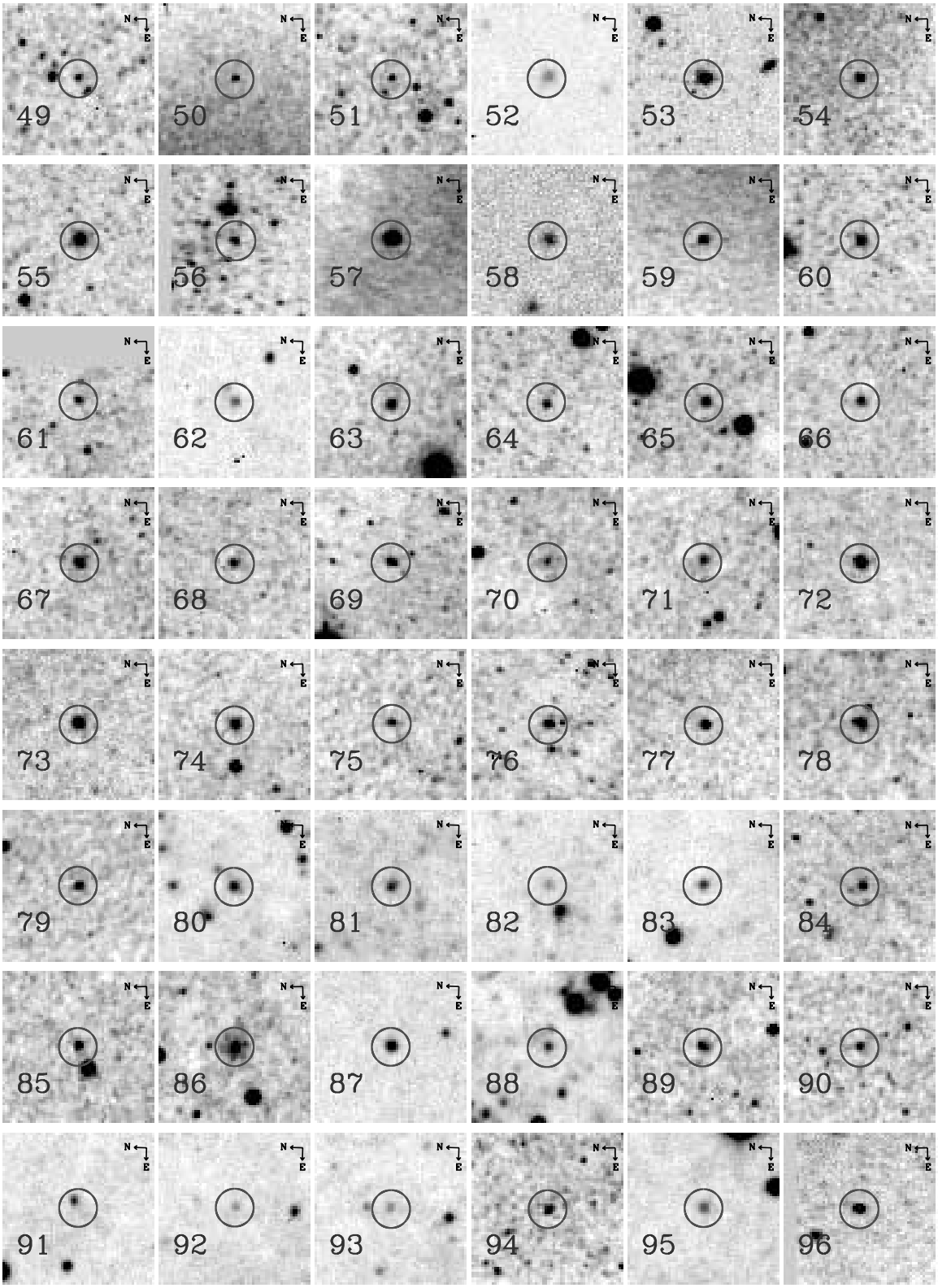

FIG. 8.—Same as Fig. 7, but for identifications from 49 to 96. [*See the electronic edition of the Journal for a color version of this figure.*]

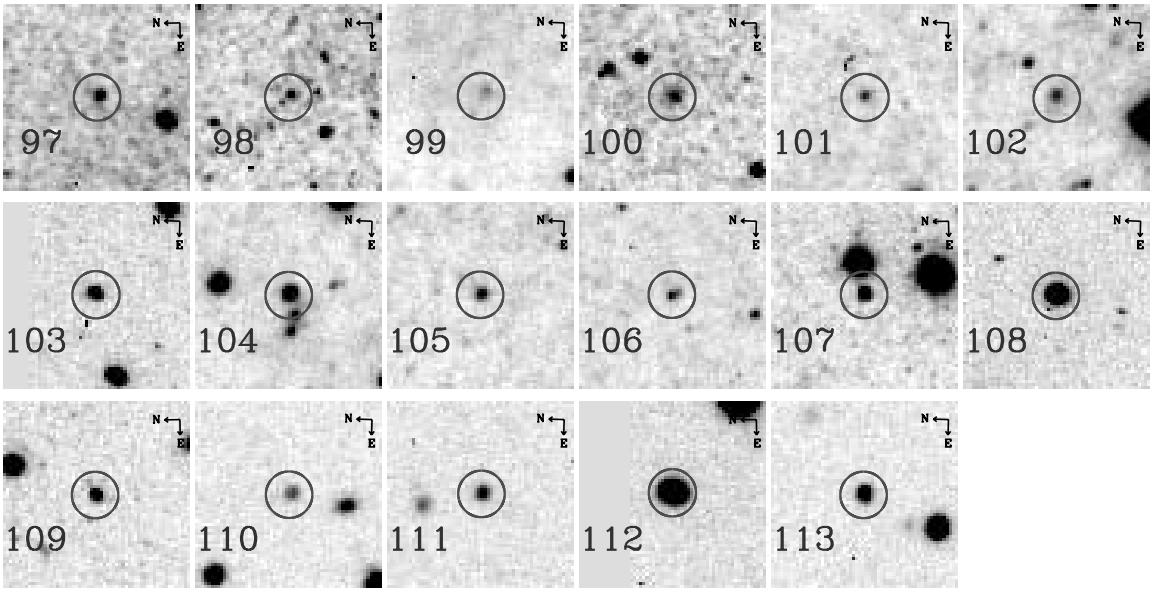

FIG. 9.—Same as Fig. 7, but for identifications from 97 to 113. [*See the electronic edition of the Journal for a color version of this figure*.]

confirmed GCs, young star clusters, foreground stars (F, G, and K types), and three galaxies (M31, M32, and a background galaxy).

The radial velocities were used as a strong constraint on the membership of the objects belonging to the Galaxy, M31, or the distant universe. Most of the objects with radial velocities less than -200 km s^{-1} are probably M31 members, while those from -200 to $+200$ km s^{-1} could be M31 members or Galactic foreground stars. We considered all the objects with $v < -300$ km s^{-1} to be M31 members. The objects with $v > 300$ km s^{-1} were classified as background galaxies. For objects with -300 km s^{-1} $< v < +300$ km s^{-1}, we classified each object consulting its spectral class.

Combining both image and spectral inspections was very efficient and accurate in classifying the objects. For our fields F08–F42, we used both image inspection and spectral inspection methods, while for the fields without spectroscopic data (F1–F7, F43–F52, and F56) we used only the image inspection method.

We have classified the final GCs/GC candidates into three classes according to probability as follows: (1) class 1, genuine GCs that were confirmed by either spectral types and radial velocities or high-resolution images (mostly *HST* images); (2) class 2, probable clusters that are probably GCs from imaging data but without spectral information; and (3) class 3, possible clusters that are possibly GCs, but may be other kinds of objects like background galaxies.

4. RESULTS

4.1. *The Catalog of New Globular Clusters in M31*

By applying the cluster search method described in the previous section to the 53 KPNO fields of M31 covering an $\sim 3^\circ \times 3^\circ$ area, we have found a total of 1164 GC candidates. Among these there are 605 new GC candidates found in this study and 559 previously known GCs in the catalogs of previous studies (e.g., Huxor et al. 2005; Galleti et al. 2006; Mackey et al. 2007).

Table 4 lists a summary of the numbers of the GCs and GC candidates for each class. Among the new 605 GC candidates there are 113 genuine GCs (class 1), 258 probable GCs (class 2), and 234 possible GCs (class 3). Among the known GCs in previous studies we find 383 genuine GCs, 109 probable GCs, and 67 possible GCs. In total there are 496 genuine GCs, 367 probable GCs, and 301 possible GCs.

Tables 5, 6, and 7 present the lists of the GCs and GC candidates newly found in this study for genuine GCs, probable GCs, and possible GCs, respectively. In these tables the columns give the running number (col. [1]), the coordinates in right ascension and declination (J2000.0; cols. [2] and [3]), T_1 magnitudes (col. [4]), $(M - T_1)$ and $(C - T_1)$ colors (cols. [5] and [6]), and

TABLE 8
A LIST OF STARS IDENTIFIED IN THIS STUDY

ID (1)	R.A. (J2000.0) (2)	Decl. (J2000.0) (3)	T_1 (4)	$(M - T_1)$ (5)	$(C - T_1)$ (6)	v (km s^{-1}) (7)
1.....	00 35 10.78	+41 44 03.1	16.340 ± 0.003	0.711 ± 0.005	1.701 ± 0.008	−15.9 ± 37.2
2.....	00 35 17.16	+41 22 13.0	16.014 ± 0.003	0.707 ± 0.004	1.669 ± 0.006	−54.5 ± 28.2
3.....	00 35 20.08	+41 21 41.7	15.935 ± 0.002	0.590 ± 0.004	1.341 ± 0.005	−1.0 ± 27.0
4.....	00 35 25.19	+42 06 51.3	16.863 ± 0.006	0.627 ± 0.009	1.344 ± 0.011	−102.1 ± 38.0
5.....	00 35 26.09	+41 44 42.0	15.639 ± 0.002	0.618 ± 0.003	1.421 ± 0.004	−66.8 ± 26.1

NOTES.—Table 8 is published in its entirety in the electronic edition of the *Astronomical Journal*. A portion is shown here for guidance regarding its form and content. Units of right ascension are hours, minutes, and seconds, and units of declination are degrees, arcminutes, and arcseconds.

TABLE 9
A List of Galaxies Identified in this Study

ID (1)	R.A. (J2000.0) (2)	Decl. (J2000.0) (3)	T_1 (4)	$(M - T_1)$ (5)	$(C - T_1)$ (6)	v (km s^{-1}) (7)	RBC2 ID[a] (8)
1.....	00 36 32.94	+40 24 52.7	16.408 ± 0.004	0.788 ± 0.006	1.849 ± 0.009	10779.3 ± 51.1	B294
2.....	00 40 15.67	+41 48 30.4	17.252 ± 0.008	0.841 ± 0.014	1.835 ± 0.022	53856.7 ± 68.2	B320
3.....	00 40 27.23	+41 29 09.1	17.352 ± 0.014	0.801 ± 0.018	1.705 ± 0.023	41878.8 ± 69.1	B007
4.....	00 40 55.18	+41 57 28.7	17.695 ± 0.011	0.881 ± 0.021	2.174 ± 0.041	35348.9 ± 74.1	...
5.....	00 41 00.13	+41 55 39.8	16.972 ± 0.006	0.951 ± 0.012	2.260 ± 0.023	28551.8 ± 65.7	...
6.....	00 42 49.35	+41 59 06.6	18.392 ± 0.032	0.732 ± 0.056	2.059 ± 0.138	35984.0 ± 100.3	...
7.....	00 43 14.56	+40 22 58.9	18.767 ± 0.028	1.004 ± 0.052	2.532 ± 0.116	38863.2 ± 89.3	...
8.....	00 43 15.67	+42 01 47.9	17.738 ± 0.018	0.759 ± 0.031	2.045 ± 0.075	22246.6 ± 58.1	...
9.....	00 43 47.30	+40 32 54.8	17.900 ± 0.011	0.986 ± 0.022	2.040 ± 0.036	52702.6 ± 99.2	...
10.....	00 44 52.40	+41 46 29.1	19.630 ± 0.095	−0.183 ± 0.112	2.849 ± 0.761	47585.2 ± 41.2	...
11.....	00 45 48.73	+41 02 14.0	17.835 ± 0.011	0.819 ± 0.020	1.939 ± 0.032	33179.9 ± 107.0	...
12.....	00 46 24.87	+41 35 09.1	17.223 ± 0.009	0.640 ± 0.013	1.385 ± 0.015	28367.1 ± 80.7	B385
13.....	00 46 29.20	+40 20 35.0	17.658 ± 0.009	0.869 ± 0.016	2.057 ± 0.029	35611.0 ± 112.8	...
14.....	00 46 43.77	+41 49 09.9	16.840 ± 0.008	1.022 ± 0.015	2.516 ± 0.039	37728.3 ± 85.9	B389
15.....	00 47 00.27	+40 59 38.0	17.011 ± 0.006	0.711 ± 0.010	1.523 ± 0.013	32027.7 ± 60.1	B299D
16.....	00 47 00.33	+40 40 36.7	17.427 ± 0.008	0.872 ± 0.015	2.078 ± 0.027	39567.8 ± 67.8	B300D
17.....	00 47 12.50	+41 30 07.7	17.880 ± 0.016	0.887 ± 0.025	2.164 ± 0.041	32632.9 ± 89.6	...
18.....	00 47 26.23	+41 47 41.4	18.634 ± 0.027	0.942 ± 0.059	2.514 ± 0.187	38498.4 ± 102.2	...
19.....	00 47 31.18	+41 52 59.7	18.501 ± 0.024	0.854 ± 0.050	2.364 ± 0.147	32383.9 ± 105.4	...
20.....	00 47 41.69	+41 46 41.4	17.518 ± 0.010	0.901 ± 0.022	2.089 ± 0.048	32408.5 ± 78.0	...
21.....	00 48 33.48	+41 43 44.4	18.070 ± 0.016	0.855 ± 0.033	2.212 ± 0.079	38208.4 ± 113.9	...

Notes.—Units of right ascension are hours, minutes, and seconds, and units of declination are degrees, arcminutes, and arcseconds.
[a] Identification in the RBC2 of Galleti et al. (2006).

the radial velocities derived in this study (col. [7]). The magnitudes and colors here are from the simple aperture photometry derived using SExtractor with an aperture of radius 5″. Figures 7, 8, and 9 show the *R*-band mosaic images of genuine GCs (class 1) with identifications in Table 5 labeled.

Tables 8 and 9 present the lists of 111 stars and 21 galaxies, respectively, identified in the present study. The columns are the same as those of Table 5, except the last column of Table 9, which gives the identification matched with the RBC2 of Galleti et al. (2006). These lists of stars and galaxies were obtained from the spectral classification described in § 3. We found that 13 objects in these lists were already identified as galaxies or GC candidates without measured velocities in the RBC2 catalog.

4.2. *Properties of New Globular Clusters*

Although the detailed properties of the newly found GCs/GC candidates, as well as those of the whole M31 GC system including the previously known GCs, will be presented in separate papers, we show a few salient features of the newly found objects here.

Figure 10 shows the T_1-$(C - T_1)$ CM diagram (Fig. 10*a*), $(C - T_1)$ color distributions (Fig. 10*b*), and T_1 LF (Fig. 10*c*) of the newly found GCs/GC candidates in Tables 5, 6, and 7. Figure 11 shows the $(C - M)$-$(C - T_1)$ CC diagram of the same objects. Most of the class 1 GCs have T_1 magnitudes of 17.5–19.5 mag, which would be $V \approx 17.9$–19.9 mag assuming $(C - T_1) \approx 1.5$ (see below) and using the Geisler's (1996) transformation coefficients between *UBVRI* photometry and CT_1 photometry. Figure 12 shows the direct comparison of the confirmed, previously known GCs and newly found, class 1 GCs in the T_1-$(C - T_1)$ CM diagram, and it is noted that most of the class 1 GCs newly found in this study are fainter than most of the confirmed, previously known GCs. The brightest object among the newly found class 1 GCs has $T_1 \sim 14.6$ mag ($V \sim 15.0$ mag), and the faintest one has $T_1 \sim 19.9$ mag ($V \sim 20.1$ mag). We checked the color distributions of the previously known GCs and newly found GCs, confirming that they are quite similar.

Figure 10*b* shows that the $(C - T_1)$ color distributions of all three classes encompass the color range of $1 < (C - T_1) < 2$

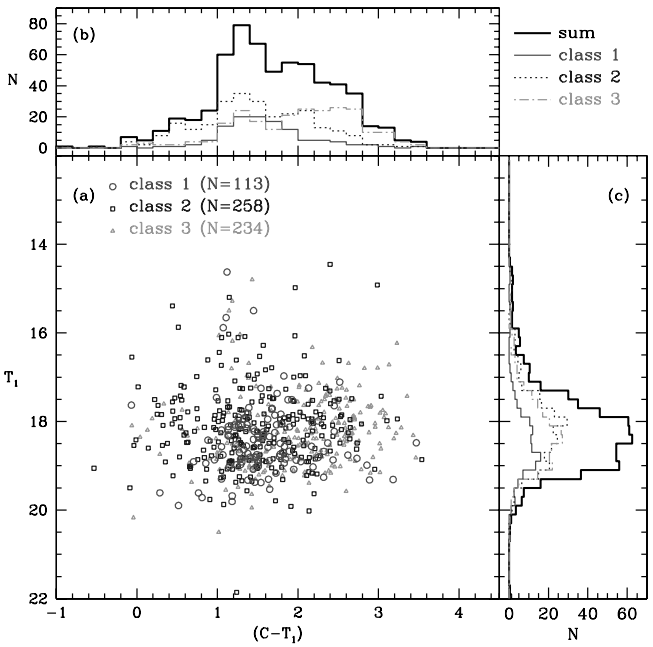

Fig. 10.—Photometric diagrams of the three classes of GCs/GC candidates newly found in this study. (*a*) T_1-$(C - T_1)$ diagram; (*b*) $(C - T_1)$ color distribution; (*c*) T_1 LF. Open circles and thin solid histograms are for genuine GCs (class 1), open squares and dotted histograms are for probable GCs (class 2), and open triangles and dot-dashed histograms are for possible GCs (class 3). Thick solid histograms in panels *b* and *c* are the sum of the numbers of all three classes. [*See the electronic edition of the Journal for a color version of this figure.*]

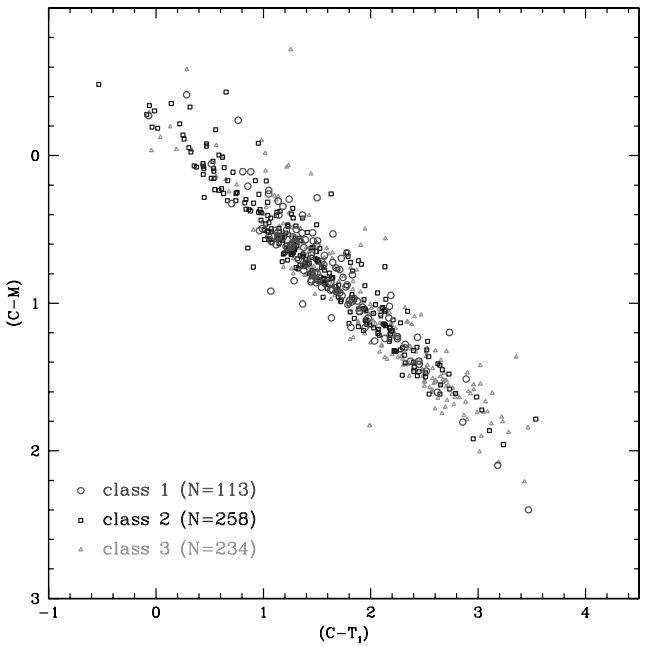

FIG. 11.—$(C - M)$-$(C - T_1)$ diagram of the three classes of GCs/GC candidates newly found in this study. Open circles are for genuine GCs (class 1), open squares are for probable GCs (class 2), and open triangles are for possible GCs (class 3). [*See the electronic edition of the Journal for a color version of this figure.*]

$[0.6 \lesssim (B - V) \lesssim 1.0$; Geisler 1996], in which most of the class 1 objects reside. There are a rather large number of very red objects with $2 < (C - T_1) < 2.5$ $[(B - V) \approx 1.0$–$1.3]$, which could be reddened GCs or intrinsically red clusters.

Figure 13 shows the spatial distribution and histograms of the newly found GCs and GC candidates. Open circles and filled histograms are for class 1 GCs in this study, crosses are for class 2 GCs in this study, and dots and open solid histograms are for GCs in the catalogs of Galleti et al. (2006, their class 1), Huxor et al. (2005), and Mackey et al. (2007). Most of the newly found, class 1

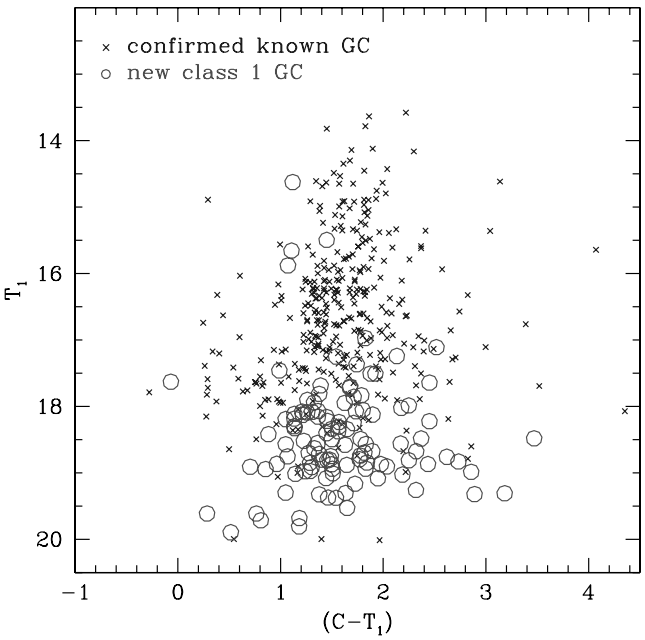

FIG. 12.—T_1-$(C - T_1)$ CM diagram of confirmed, previously known GCs in Fig. 3*a* (*crosses*) and newly found, class 1 GCs in Fig. 10*a* (*open circles*). [*See the electronic edition of the Journal for a color version of this figure.*]

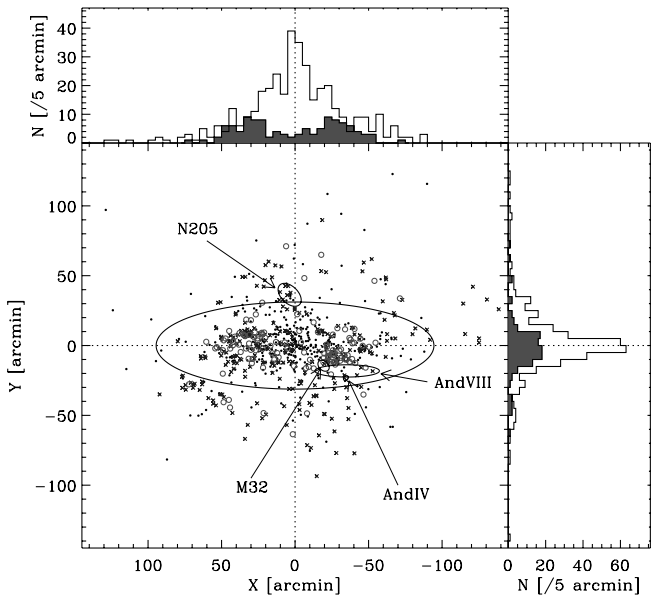

FIG. 13.—Spatial distribution and histograms of the newly found GCs and GC candidates. Here X is the distance measured parallel to the major axis of M31, increasing to the northeast direction, and Y is the distance parallel to the minor axis. The large ellipse is for M31 with position angle 37.7° (Racine 1991). The positional data of the galaxies are from Karachentsev et al. (2004), while those for And VIII are from Morrison et al. (2003). Open circles are for class 1 GCs in this study, crosses are for class 2 GCs in this study, and dots are for GCs in the catalogs of Galleti et al. (2006; their class 1), Huxor et al. (2005), and Mackey et al. (2007). The filled histograms are for class 1 GCs in this study, and the open solid histograms are for GCs in the three papers above. [*See the electronic edition of the Journal for a color version of this figure.*]

GCs are located in the disk area of M31. Higher spatial resolution imaging and spectroscopy, and possibly in the near-infrared wavelength band, would be needed to search for GCs in the central region of M31 where we missed many faint GCs, as seen in Figure 13 (*top*).

5. SUMMARY

We have presented the results of a new systematic wide-field CCD survey of M31 GCs. Using Washington CMT_1 CCD images obtained at the KPNO 0.9 m telescope and spectra obtained using the WIYN 3.5 m telescope and Hydra multifiber bench spectrograph, we have investigated the photometric and morphological parameters of the objects, visually checked their images, and obtained their spectra and radial velocities. Finally, we have found 1164 GCs and GC candidates, of which 559 are previously known GCs and 605 are newly found GC candidates. Among the new objects there are 113 genuine GCs (class 1), 258 probable GCs (class 2), and 234 possible GCs (class 3). Among the previously known objects there are 383 genuine GCs, 109 probable GCs, and 67 possible GCs. In total there are 496 genuine GCs, 367 probable GCs, and 301 possible GCs.

The magnitudes and colors of most of the newly found class 1 objects are 17.5 mag $< T_1 <$ 19.5 mag and $1 < (C - T_1) < 2$. The faintest part of the M31 GC LF is mostly filled with these new GC candidates, although the intrinsically very faint GCs like AM 4, Palomar 1, E3, and Palomar 13 in the Galaxy (see, e.g., van den Bergh & Mackey 2004; Sarajedini et al. 2007) may remain to be detected.

We would like to thank the anonymous referee for providing prompt and thoughtful comments that helped improve the original

manuscript. The authors are grateful to the staff members of the KPNO for their warm support during our observations and data reduction. The WIYN Observatory is a joint facility of the University of Wisconsin–Madison, Indiana University, Yale University, and the National Optical Astronomy Observatory. M. G. L. was supported in part by a Korean Research Foundation grant (KRF-2000-DP0450) and ABRL (R14-2002-058-01000-0). D. G. gratefully acknowledges support from Chilean Centro de Astrofísica FONDAP grant 15010003. A. S. was supported by NSF CAREER grant AST 00-94048.

REFERENCES

Alloin, D., Pelat, D., & Bijaoui, A. 1976, A&A, 50, 127 (erratum 54, 321 [1977])
Aurière, M., Coupinot, G., & Hecquet, J. 1992, A&A, 256, 95
Baade, W., & Arp, H. C. 1964, ApJ, 139, 1027
Barmby, P., & Huchra, J. P. 2001, AJ, 122, 2458
Barmby, P., Huchra, J. P., Brodie, J. P., Forbes, D. A., Schroder, L. L., & Grillmair, C. J. 2000, AJ, 119, 727
Battistini, P., Bònoli, F., Braccesi, A., Federici, L., Fusi Pecci, F., Marano, B., & Börngen, F. 1987, A&AS, 67, 447
Battistini, P., Bònoli, F., Casavecchia, M., Ciotti, L., Federici, L., & Fusi Pecci, F. 1993, A&A, 272, 77
Bertin, E., & Arnouts, S. 1996, A&AS, 117, 393
Crampton, D., Cowley, A. P., Schade, D., & Chayer, P. 1985, ApJ, 288, 494
De Angeli, F., Piotto, G., Cassisi, S., Busso, G., Recio-Blanco, A., Salaris, M., Aparicio, A., & Rosenberg, A. 2005, AJ, 130, 116
Galleti, S., Federici, L., Bellazzini, M., Buzzoni, A., & Fusi Pecci, F. 2006, A&A, 456, 985
Galleti, S., Federici, L., Bellazzini, M., Fusi Pecci, F., & Macrina, S. 2004, A&A, 416, 917
Geisler, D. 1996, AJ, 111, 480
Hubble, E. P. 1932, ApJ, 76, 44
Huchra, J. P., Brodie, J. P., & Kent, S. M. 1991, ApJ, 370, 495
Huxor, A. P., Tanvir, N. R., Irwin, M. J., Ibata, R., Collett, J. L., Ferguson, A. M. N., Bridges, T., & Lewis, G. F. 2005, MNRAS, 360, 1007
Karachentsev, I. D., Karachentseva, V. E., Huchtmeier, W. K., & Makarov, D. I. 2004, AJ, 127, 2031
Kim, S. C., Lee, M. G., Geisler, D., Seguel, J., Sarajedini, A., & Harris, W. E. 2002, in IAU Symp. 207, Extragalactic Star Clusters, ed. D. Geisler, E. K. Grebel, & D. Minniti (San Francisco: ASP), 143
Kodaira, K., Vansevicius, V., Bridzius, A., Komiyama, Y., Miyazaki, S., Stonkute, R., Sabelviciute, I., & Narbutis, D. 2004, PASJ, 56, 1025
Lee, M. G., Kim, S. C., Geisler, D., Seguel, J., Sarajedini, A., & Harris, W. E. 2002, in IAU Symp. 207, Extragalactic Star Clusters, ed. D. Geisler, E. K. Grebel, & D. Minniti (San Francisco: ASP), 46
Mackey, A. D., et al. 2006, ApJ, 653, L105
———. 2007, ApJ, 655, L85
Martin, N. F., Ibata, R. A., Irwin, M. J., Chapman, S., Lewis, G. F., Ferguson, A. M. N., Tanvir, N., & McConnachie, A. W. 2006, MNRAS, 371, 1983
Mayall, N. U., & Eggen, O. J. 1953, PASP, 65, 24
Mochejska, B. J., Kaluzny, J., Krockenberger, M., Sasselov, D. D., & Stanek, K. Z. 1998, Acta Astron., 48, 455
Morrison, H. L., Harding, P., Hurley-Keller, D., & Jacoby, G. 2003, ApJ, 596, L183
Perrett, K. M., Bridges, T. J., Hanes, D. A., Irwin, M. J., Brodie, J. P., Carter, D., Huchra, J. P., & Watson, F. G. 2002, AJ, 123, 2490
Racine, R. 1991, AJ, 101, 865
Salaris, M., & Weiss, A. 2002, A&A, 388, 492
Santos, J. F. C., Jr., Alloin, D., Bica, E., & Bonatto, C. 2002, in IAU Symp. 207, Extragalactic Star Clusters, ed. D. Geisler, E. K. Grebel, & D. Minniti (San Francisco: ASP), 727
Sarajedini, A., et al. 2007, AJ, 133, 1658
Sargent, W. L. W., Kowal, C. T., Hartwick, F. D. A., & van den Bergh, S. 1977, AJ, 82, 947
Seguel, J., Geisler, D., Lee, M. G., Kim, S. C., Sarajedini, A., & Harris, W. E. 2002, in IAU Symp. 207, Extragalactic Star Clusters, ed. D. Geisler, E. K. Grebel, & D. Minniti (San Francisco: ASP), 146
Seyfert, C. K., & Nassau, J. J. 1945, ApJ, 102, 377
Strom, K. M. 1977, Standard Stars for IIDS Observations (Tucson: KPNO)
Tonry, J. T., & Davis, M. 1979, AJ, 84, 1511
Valdes, F. 1995, Guide to the HYDRA Reduction Task DOHYDRA (Tucson: NOAO), ftp://ftp.noao.edu/iraf/iraf/docs/dohydra.ps.Z
van den Bergh, S., & Mackey, A. D. 2004, MNRAS, 354, 713
Vetešnik, M. 1962, Bull. Astron. Inst. Czech, 13, 180
Wirth, A., Smarr, L. L., & Bruno, T. L. 1985, ApJ, 290, 140